Octupole deformation of nuclei near the spherical closed-shell configurations

Ken-ichiro Arita*
Department of Physics, Nagoya Institute of Technology, Nagoya 466-8555, Japan

(Received 2 March 2023; revised 1 May 2023; accepted 9 June 2023; published 5 July 2023)

The origin of octupole deformation for even-even nuclei near the doubly closed shell configurations are investigated by means of the semiclassical periodic orbit theory. In order to focus on the change of shell structure due to deformation, a simple infinite-well potential model is employed with octupole shape parametrized by merging a sphere and a paraboloid. Attention is paid to the contributions of the degenerate families of periodic orbits (POs) confined in the spherical portion of the potential, that are expected to partially preserve the spherical shell effect up to considerably large value of the octupole parameter. The contribution of those POs to the semiclassical trace formula plays an important role in bringing about shell energy gain due to octupole deformation in the system with a few particles added to spherical closed-shell configurations.

DOI: 10.1103/PhysRevC.108.014303

I. INTRODUCTION

Atomic nuclei take various shapes with varying numbers of constituent protons and neutrons, and the single-particle shell structures play the essential role in their deformations and shape stabilities. In general, systems with particle numbers sufficiently far from the spherical magic numbers will deform. The majority of the ground-state shapes are known to be quadrupole type, but some exotic shapes are found depending on the combinations of proton and neutron numbers, and the possible breaking of the reflection symmetry is one of the fundamental problems in nuclear structure physics. The ground-state octupole deformations are observed only for a few nuclei, such as those around the neutron-rich Ba region and Ra-Th region. These regions are located in the "north-eastern" neighbors of doubly magic nuclei on the (N, Z) plane of the nuclear chart; namely, they correspond to the systems with a few particles added to spherical closed-shell configurations [1]. Possible static octupole shapes for even-even nuclei have been systematically investigated with various theoretical approaches such as microscopic-macroscopic models [2], the generator coordinate method [3], density functional theories [4,5], and recently with the Hartree-Fock-BCS model with three-dimensional Cartesian mesh representation [6], which are consistent with the experimental data and suggest promising regions of nuclei where octupole deformation might be found.

As the origin of the ground-state octupole deformations for these nuclei, the octupole correlation within the approximately degenerate $\Delta l = 3$ pair of single-particle levels is considered to play a significant role. Such pairs of levels arise systematically above the spherical shell gaps for systems with sharp surface potential. For example, $(2g_{7/2}, 1j_{15/2})$ orbitals above the $N(Z) = 126$ gap and $(2f_{5/2}, 1i_{13/2})$ orbitals above the $N(Z) = 82$ gap are approximately degenerate in the realistic nuclear mean field potential.

Figure 1 compares the single-particle spectra of the spherical harmonic-oscillator (HO) potential model and the spherical infinite-well potential (cavity) model, which have been referred to as schematic models for light and heavy nuclei, respectively. In the cavity model, one finds pairs of $\Delta l = 3$ levels (enclosed by braces) above each shell gap, for instance, $2g$ and $1j$ levels above the $N = 138$ gap, $2f$ and $1i$ levels above the $N = 92$ gap. Thus, the cavity potential preserves important features of the shell structure of the realistic nuclear mean field, although the magic numbers are a little shifted from those of the realistic ones due to the absence of spin-orbit coupling.

Since one has large octupole matrix elements between such $\Delta l = 3$ levels, one of the levels is expected to go down rapidly with increasing octupole deformation, and the system just above the closed-shell configuration which occupies this downward level would prefer octupole shape [1]. The behavior of those levels with respect to perturbations of the octupole operators and their relation to the octupole deformation energy have been examined in Refs. [7,8].

On the other hand, from the view point of the shell correction method, shell energy is governed by the gross shell structure [9] and it is not obvious whether the origin of total shell energy can be attributed to the behavior of specific orbitals. Moreover, there must be some simple mechanism involved in the remarkable systematics in the distribution of reflection asymmetry on the nuclear chart found in the above numerical calculations.

In this paper, I analyze a simple cavity potential model to reveal the essential mechanism of the nuclear octupole deformation. As well as the behavior of $\Delta l = 3$ pairs of single-particle levels, I shall consider the effect of gross shell structure from a semiclassical point of view; namely, I examine the role of the classical periodic orbits (POs) in the semiclassical single-particle level density.

*arita@nitech.ac.jp

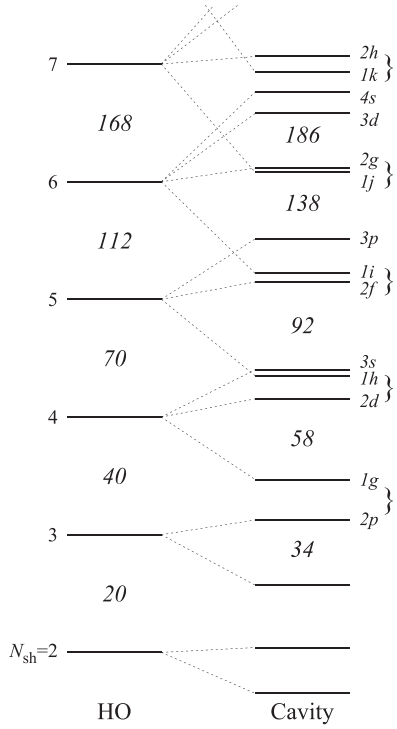

FIG. 1. Comparison of the single-particle spectra for spherical harmonic oscillator (HO) potential model (left) and spherical infinite-well (cavity) potential model (right). Nearly degenerate $\Delta l = 3$ pairs of the single-particle levels in the cavity model are indicated by braces. The italic numbers marked on each energy gap represent the number of levels below the gap, taking spin degeneracy into account.

The idea of this work was brought about by my recent works with my colleagues, in which we discussed the deformed shell effect of nuclei through the fission path [10–12]. In the fission process, a nucleus is elongated and a neck is formed which gradually separates the system into two subsystems. Such subsystems are called *prefragments*. The prefragment shell effect, associated with each of the subsystems, is expected to come up after the neck formation [13,14], and it must be playing a significant role in determining the fission path in the deformation space and the resulting fragment mass distribution. However, it is usually difficult to extract the prefragment effect alone out of the total shell effect since most of the single-particle wave functions are not localized in each of the prefragments. To deal with this problem, we have proposed a simple idea using the semiclassical periodic orbit theory (POT) [11]. In the semiclassical trace formula, shell energy is expressed as the sum over contributions of classical POs. When the neck is formed, one has families of POs confined in each of the prefragments, and their contributions to the level density can be regarded as the prefragment shell effect. The POs in the spherical (but truncated) prefragment make a strong shell effect similar to (but a little smaller than) that for a full spherical potential. Since the POs with the same property have the same kind of contribution to the shell energy, the prefragment PO should bring about considerable shell-energy gain to the system when the size of the prefragment is same as that of the spherical magic nucleus. Such a condition for the sizes of prefragments is favored by the nucleus in the fission process, and this provides a simple and intuitive explanation for the mechanism of the asymmetric fission in actinide nuclei. Although the cavity model employed in the above work is unrealistic, especially just before the scission point for instance, the essential mechanism for the prefragment shell effect will be applicable in more realistic situations. In the realistic density functional theory calculation, it has been shown that the nucleon distributions in the prefragments for the fissioning nucleus are very similar to those of isolated nuclei [15,16]. Then, one expects the same mean field in a prefragment as that for an isolated nucleus, and the semiclassical mechanism of the prefragment shell effect associated with the classical POs localized in the prefragment seems to be justified. One can expect the same situation in nuclei just above the spherical shell closures.

Thus, the main issue of this paper is to show that the above idea of the prefragment shell effect can be also used in explaining the systematics of the octupole deformation. For this aim, I employ a simple cavity potential model whose surface shape is made of a sphere and a paraboloid joined together. In the study of octupole deformation, the surface shape is usually expanded in terms of spherical harmonics Y_{lm} for convenience [2,17]. On the other hand, the way of introducing reflection asymmetry in this work is based on the physical insight that the nucleus would have shell energy gain associated with the spherical subsystem, in the same way as the strongly deformed nuclei in the fission processes. The comparison of this parametrization with the conventional one is made in the separate paper [18].

Apart from the above objective, I would also like to consider two other problems using this model. The first is to answer the question whether the octupole deformation of the cavity boundary causes the parity mixing of approximately degenerate $\Delta l = 3$ levels in the same way as the perturbation of the potential by the octupole operator. It is a nontrivial question which cannot be simply answered by the ordinary method of perturbation. The second is to confirm the validity of the semiclassical trace formula for the truncated spherical cavity which I have developed [10].

This paper is organized as follows. In Sec. II, the octupole cavity potential model employed in this work is defined, and details of the shape parametrization are discussed. Then, I investigate the parity mixing of the $\Delta l = 3$ pair of single-particle levels. Next, in Sec. III, I consider the evolution of gross shell structure with increasing octupole deformation, and its role in explaining the systematics of the octupole deformation is analyzed with the use of the semiclassical POT. Section IV is devoted to the summary and concluding remarks.

II. OCTUPOLE CORRELATION BETWEEN THE $\Delta l = 3$ PAIR OF LEVELS

As illustrated in Fig. 2, octupole deformation can be induced by pinching one spot on the surface of the sphere. Here, I shall use the term "octupole deformation" symbolically as the shape with finite octupole moment. In general, expansion

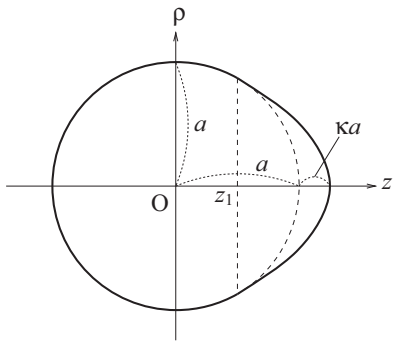

FIG. 2. Shape of the octupole surface defined by Eq. (1). A sphere and a paraboloid are smoothly joined at $z = z_1$. The relative size of the tip part κ is considered as the octupole parameter.

of the reflection-asymmetric nuclear surface shape into the spherical harmonics can contain higher order multipole components (Y_{lm} with $l > 3$) but the main reflection-asymmetric component must be Y_{3m}. I shall parametrize the axially symmetric octupole shape by merging a sphere and a paraboloid. Then, the surface $\rho = \rho_s(z)$ in the cylindrical coordinate (ρ, φ, z) is expressed as

$$\rho_s^2(z) = \begin{cases} a^2 - z^2, & -a \leqslant z \leqslant z_1, \\ 2z_1[(1+\kappa)a - z], & z_1 \leqslant z \leqslant (1+\kappa)a, \end{cases}$$
$$z_1 = (1 + \kappa - \sqrt{(2+\kappa)\kappa})a \tag{1}$$

where the sphere and the paraboloid are smoothly merged at $z = z_1$. The thickness κ ($\geqslant 0$) of the paraboloid "tip" relative to the radius a of the sphere part can be regarded as the octupole parameter. The parameter a is determined so that the volume conservation condition is satisfied. Such shape parametrization is initiated to obtain a shell effect originated from the contribution of classical PO families confined in the spherical subsystem.

Let us first look at the single-particle shell structure in the above octupole-deformed infinite-well potential

$$V(\boldsymbol{r}) = \begin{cases} 0, & [\rho(z) \leqslant \rho_s(z)], \\ +\infty, & [\rho(z) > \rho_s(z)]. \end{cases} \tag{2}$$

Figure 3 shows the single-particle level diagram plotted against the octupole parameter κ. The eigenvalue problem for the Laplace equation with Dirichlet boundary condition can be solved, e.g., by the method described in Ref. [19], which has been taken here. At above each of the spherical gaps such as $N = 92$ and 138, one may find the levels rapidly go down with increasing κ. Let us examine the reasons of such behavior. The most rapidly decreasing level above the $N = 92$ (138) gap is the $2f$ ($1j$) orbitals with the magnetic quantum number $K = 0$, and there are $\Delta l = 3$ orbitals $1i$ ($2g$) just above it (see also Fig. 1). These pairs are indicated by the thick broken curves in Fig. 3. Thus, the above behavior of the levels seems to be related to the parity mixing of those levels due to the octupole correlation.

Here let us review some basics on the breaking of reflection symmetry and parity mixing. Suppose that two levels $|1\rangle$ and $|2\rangle$ with opposite parities are approximately degenerate in the

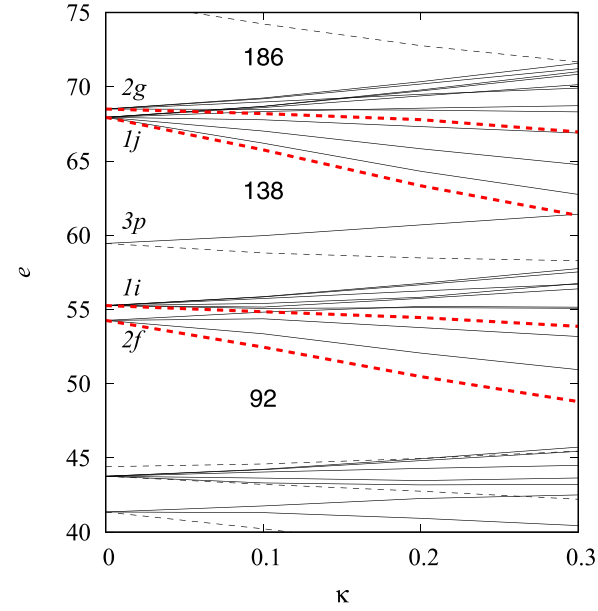

FIG. 3. Single-particle level diagram. Broken and solid curves represent $K = 0$ and $K \geqslant 1$ levels, respectively. Thick broken curves represent the pairs of $\Delta l = 3$ levels with $K = 0$ that are approximately degenerate in the spherical limit $\kappa = 0$.

symmetric limit:

$$H_0|1\rangle = (\varepsilon - \delta)|1\rangle, \quad H_0|2\rangle = (\varepsilon + \delta)|2\rangle \quad (\delta > 0),$$
$$P|1\rangle = \sigma|1\rangle, \quad P|2\rangle = -\sigma|2\rangle \quad (\sigma = \pm 1), \tag{3}$$

where P is the parity (space inversion) operator and H_0 is the reflection-symmetric Hamiltonian ($H_0 P = P H_0$). Consider the parity-violating perturbation λV ($PV = -VP$) which satisfies $\langle 1|V|1\rangle = \langle 2|V|2\rangle = 0$ and $\langle 1|V|2\rangle = \langle 2|V|1\rangle = v > 0$. Then, the parity mixing is described by the 2×2 Hamiltonian matrix

$$H = H_0 + \lambda V = \begin{pmatrix} \varepsilon - \delta & \lambda v \\ \lambda v & \varepsilon + \delta \end{pmatrix}. \tag{4}$$

The solutions of the eigenvalue equation $H|\psi_\pm\rangle = E_\pm|\psi_\pm\rangle$ are given by

$$E_\pm(\lambda) = \varepsilon \pm \sqrt{\delta^2 + (\lambda v)^2}, \tag{5}$$

$$|\psi_-(\lambda)\rangle = C\left(|1\rangle - \frac{\lambda v}{\sqrt{\delta^2 + (\lambda v)^2} + \delta}|2\rangle\right),$$
$$|\psi_+(\lambda)\rangle = C\left(|2\rangle + \frac{\lambda v}{\sqrt{\delta^2 + (\lambda v)^2} + \delta}|1\rangle\right), \tag{6}$$

where C is the normalization constant. The parity doublet $|1\rangle$ and $|2\rangle$ gradually mix and the energy splitting grows with increasing λ. Finally, for $\lambda v \gg \delta$, complete mixing is achieved and one has the parity partner

$$|\psi_\pm\rangle \simeq \frac{1}{\sqrt{2}}(|1\rangle \pm |2\rangle), \quad P|\psi_\pm\rangle \simeq \sigma|\psi_\mp\rangle, \tag{7}$$

where the energy splitting is given approximately by

$$\Delta E \sim 2\lambda v. \tag{8}$$

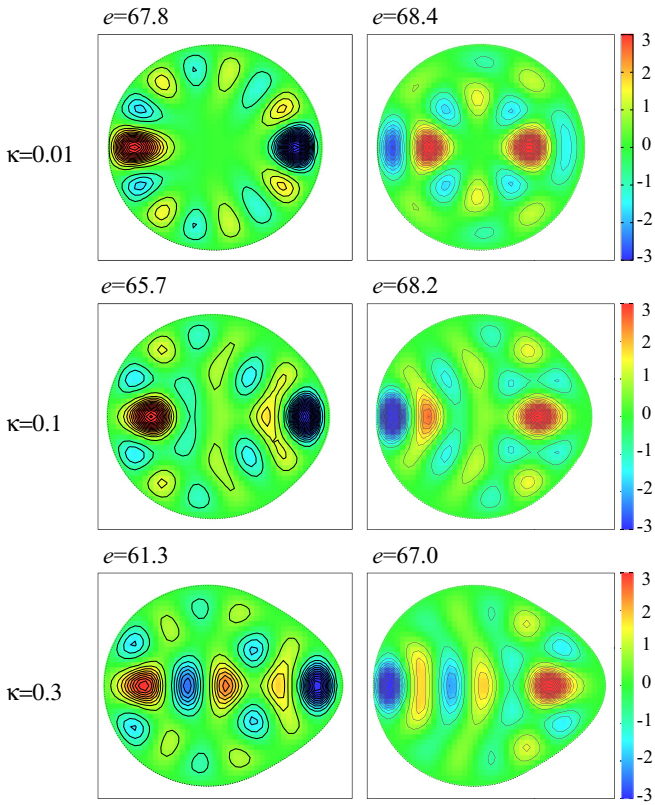

FIG. 4. Evolution of the wave functions of the $\Delta l = 3$ pair of single-particle levels just above the $N = 138$ gap. The contour plots of the wave functions are shown. The energy eigenvalue e of each level is given at the upper left of the figure. The panels in the left and right columns are for the lower and upper levels, originating from the negative-parity $1j$ and positive-parity $2g$ orbitals, respectively, with increasing octupole parameter κ from top to bottom.

The question here is whether the changes in wave functions and eigenvalue energies as described above also apply to the cavity model against octupole deformation of the potential surface. Figure 4 displays the evolutions of the wave functions of a pair of single-particle levels with increasing κ for the $K = 0$ states originated from the $\Delta l = 3$ orbital pair $1j$ and $2g$ just above the spherical gap $N = 138$. Each panel shows the contour plot of the wave function. At $\kappa = 0.01$, each wave function is almost entirely occupied by the parity eigenstate. With increasing octupole deformation, a complete mixing seems to be achieved already at $\kappa \approx 0.1$, where one of the wave functions is quite similar to a space inversion of the other as shown in the second equation of (7). The behavior of the energy splitting with increasing κ is also consistent with Eq. (8) by assuming $\lambda \propto \kappa$. The same properties also hold for the $K > 0$ pairs of levels. Thus, it is confirmed that the parity mixing of nearly degenerate $\Delta l = 3$ levels explains the behavior of the single-particle shell structure against the octupole deformation. This behavior is expected to play a certain role in enabling the system to achieve stable octupole deformation.

III. GROSS SHELL STRUCTURE IN TERMS OF CLASSICAL PERIODIC ORBITS

The liquid drop model explains an average property of nuclei, and the quantum fluctuation about it is essentially given by the single-particle shell effect. In a liquid drop picture, a nucleus is most stable in the spherical shape, which minimizes the surface energy. The pronounced shell structure in the spherical potential is advantageous for the closed-shell configurations, and conversely, disadvantageous for the open-shell configurations. The spherical shape becomes more unstable as the number of particles deviates from any magic number corresponding to the closed-shell configuration, and the system will deform when the shell energy gain due to the deformation surpasses the increase of liquid-drop surface energy.

The nuclear ground-state deformations are considered to be of the quadrupole type in most cases. Another reason why the quadrupole type deformation is most likely to occur is the regularity of single-particle motion, which contributes to the strong deformed shell effect. In a potential with small quadrupole deformation, classical motion of a single particle is mostly regular (stable). However, the classical motion rapidly becomes chaotic (unstable) with increasing octupole-type deformation [20]. In general, quantum level repulsion occurs in a classically chaotic system, which makes the shell effect small compared to systems where the classical motion is regular. For an exotic deformation to emerge, a considerably strong shell effect is necessary, which is usually associated with dynamical symmetries, or resonances in another word, arising locally in the system for specific potential shapes [21–23]. A typical example is the so-called superdeformed state, where the axis ratio is approximately 2:1. It is understood in analogy with the pronounced degeneracy of levels found in a deformed oscillator potential with rational axis ratio.

In analyzing the origin of such gross shell effect, semiclassical POT provides us with a powerful tool [23–27]. In general, distribution of single-particle energy eigenvalues shows a regular oscillating pattern, but its origin cannot be explained within the framework of pure quantum mechanics. To describe the above oscillation, Balian and Bloch considered a semiclassical approximation and derived an outstanding formula which expresses the quantum level density

$$g(e) = \sum_i \delta(e - e_i) \tag{9}$$

as the sum over contributions from the classical POs [25]. The formula they have obtained is specific to the infinite-well (cavity) potential systems, although it is applicable to any dimension and shape. Independently of them, Gutzwiller derived the same type of the formula from a different semiclassical approach [24]. His formula, known as the Gutzwiller trace formula, can be applied to Hamiltonian systems with more generic potentials, but is limited to the case where all classical motions are unstable and the system has no continuous symmetries such as rotational symmetries. In the opposite extreme with respect to the stability of the classical motions, the trace formulas for completely integrable (multiply periodic) systems are derived by Berry and Tabor based on the

torus quantization condition of Einstein, Brillouin, and Keller (EBK) [28]. The extension of the Gutzwiller trace formula to a system with continuous symmetries was made, e.g., in Refs. [9,29]. The formulas applicable to the stable orbits that encounter bifurcations, for which Gutzwiller's formula breaks down, have been derived by uniform approximations [30] and the improved stationary-phase approximation [31,32]. The general version of the trace formula, incorporating all the above, might be expressed as

$$g(e) = g_0(e) + \delta g(e), \tag{10}$$

$$\delta g(e) \simeq \sum_{\rm PO} A_{\rm PO}(e) \cos\left(\frac{1}{\hbar} S_{\rm PO}(e) - \frac{\pi}{2}\mu_{\rm PO}\right), \tag{11}$$

where g_0 represents the average level density, equivalent to the (extended) Thomas-Fermi approximation [26,33,34], and the oscillating component δg is expressed as the sum over the contribution of classical POs. $S_{\rm PO} = \oint_{\rm PO} \boldsymbol{p} \cdot d\boldsymbol{r}$ represents the action integral along the PO, $\mu_{\rm PO}$ is the Maslov index related to the geometrical character of PO, and the amplitude $A_{\rm PO}$ is fully determined by the classical properties (such as degeneracy, period, and stability) of the orbit. Since the action integral is generally a monotonically increasing function of energy e, each contribution of PO in the right-hand side of Eq. (11) gives a regularly oscillating function of e. The orbit with shorter period $T_{\rm PO} = dS_{\rm PO}/de$ gives the gross structure of the level density and the longer orbits contribute to the finer structures. In order to investigate the gross shell structure, it is sufficient to consider the contributions of only a few shortest POs. If the single-particle Hamiltonian has continuous symmetries, each PO generally forms a continuous family of several parameters. Such a family is called a degenerate orbit and the number of continuous parameters $\mathcal{K}_{\rm PO}$ for the family is called the degeneracy. Note that the orbits with higher degeneracies make a more significant contribution to the level density. Speaking in the context of semiclassical $\hbar$ expansion, the amplitude factor $A_{\rm PO}$ is of the order $\hbar^{-\mathcal{K}_{\rm PO}/2}$.

Looking at the level diagram in Fig. 3, one will find an approximately degenerate cluster of levels below each spherical shell gap, preserving strong shell effects up to fairly large values of the octupole parameter κ. As I show in the following, this strong shell effect under octupole deformation is related to the local symmetry of the system, namely, the presence of the partially spherically symmetric subsystem. In the smooth potential models, dynamical symmetries play the same role. If the system has such special local symmetry or dynamical symmetry under the exotic shape, a strong deformed shell effect is expected and the importance of such shape degree of freedom might come into competition with that of the quadrupole type.

Among the classical POs in the cavity model under consideration, there are degenerate family of orbits localized in the sphere part of the potential. Figure 5 displays some short simple POs. The upper panels show the diameter ($\mathcal{K} = 2$) and regular polygon ($\mathcal{K} = 3$) families of orbits localized in the spherical part, and the lower panels show the isolated ($\mathcal{K} = 0$) linear symmetry-axis orbit and the meridian-plane orbit families ($\mathcal{K} = 1$). There are also three-dimensional (nonplanar)

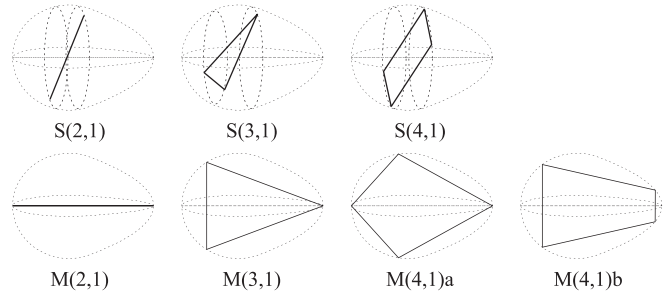

FIG. 5. Some short classical POs in the octupole cavity whose surface is given by Eq. (1) with the octupole parameter $\kappa = 0.2$. The lower panels represent the meridian-plane orbits $M(v, w)$, and the upper panels represent the regular polygon orbit families $S(v, w)$ confined in the sphere part of the potential. The indices v and w represent the number of vertices and the winding number, respectively.

orbits that form $\mathcal{K} = 1$ families, but they are longer than the above ones and contribute only to the finer shell structures.

One can see the contribution of these orbits to the semiclassical level density using the Fourier transformation technique. Through the classical motion of the particle in the cavity potential, the magnitude of the momentum p is kept constant, and the action integral along the orbit is simply given by the product of p and the geometric length $L_{\rm PO}$ of the orbit. Thus, the level density in the wave-number variable k ($p = \hbar k$) is expressed as

$$\begin{aligned} g(k) &= g(e)\frac{de}{dk} \\ &= g_0(k) + \sum_{\rm PO} a_{\rm PO}(k) \cos\left(kL_{\rm PO} - \frac{\pi}{2}\mu_{\rm PO}\right). \end{aligned} \tag{12}$$

The simple k dependence of the above phase factor enables us to estimate the contribution of each orbit by the Fourier transformation of level density. Let us consider the Fourier transform defined by

$$F(L) = \sqrt{\frac{\pi}{2}}\frac{1}{k_c}\int g(k) e^{ikL} e^{-(k/k_c)^2/2} dk. \tag{13}$$

In this definition, a Gaussian cutoff factor is incorporated into the integrand in order to exclude the high energy part ($k \gg k_c$) of the level density which is numerically inaccessible. The calculation of the Fourier transform of the exact quantum level density is straightforward if one has the quantum energy spectrum $\{e_j = (\hbar k_j)^2/2m\}$. Inserting $g(k) = \sum_j \delta(k - k_j)$ into Eq. (13), one has

$$F^{(\rm qm)}(L) = \sqrt{\frac{\pi}{2}}\frac{1}{k_c}\sum_j e^{ik_jL} e^{-(k_j/k_c)^2/2}. \tag{14}$$

On the other hand, by inserting the semiclassical expression (12) into (13), one has

$$F^{(\rm cl)}(L) = F_0(L) + \sum_{\rm PO} a_{\rm PO} e^{-i\pi\mu_{\rm PO}/2} e^{-\{k_c(L-L_{\rm PO})\}^2/2}, \tag{15}$$

which is a function exhibiting peaks at the lengths of the POs, $L = L_{\rm PO}$, with heights proportional to the amplitude $a_{\rm PO}$. In deriving Eq. (15), k dependence of the amplitude $a_{\rm PO}$

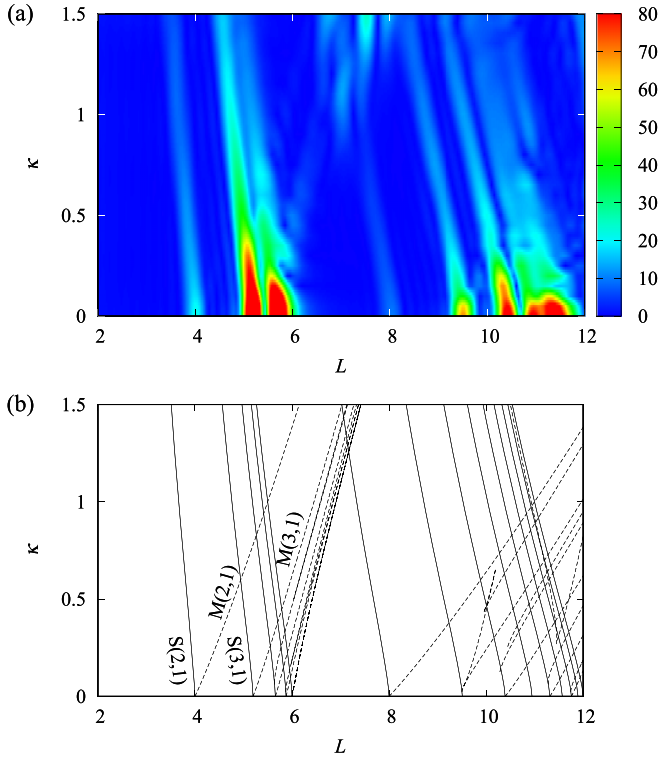

FIG. 6. In the upper panel (a), modulus of the Fourier transform of the quantum level density $|F^{(\mathrm{qm})}(L;\kappa)|$ [see Eq. (14)] is shown as a function of L and κ. In the lower panel (b), lengths of the classical POs are plotted as functions of κ. Solid lines represent the lengths of the regular polygon orbits confined in the sphere part, and the broken lines are for the meridian-plane orbits.

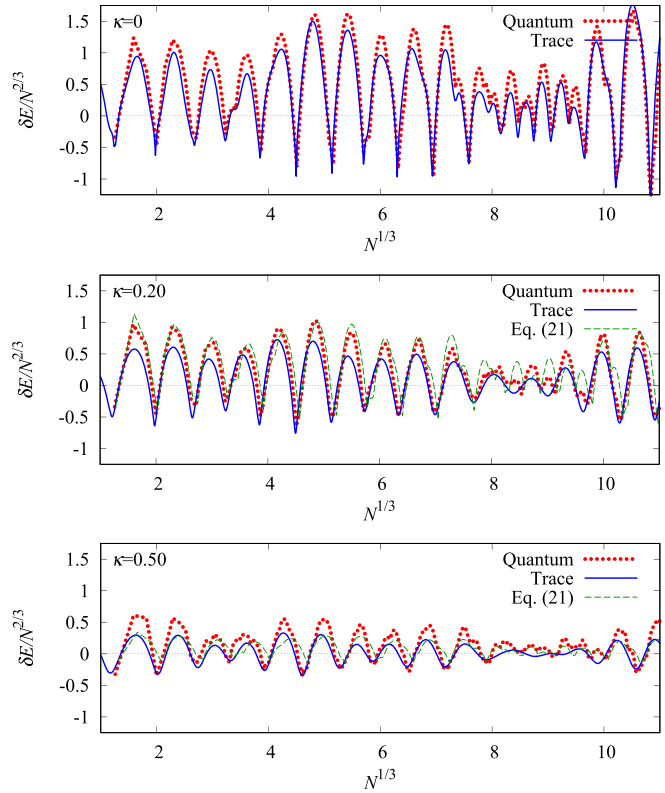

FIG. 7. Shell energy $\delta E(N)$ multiplied by $N^{-2/3}$ plotted against $N^{1/3}$, for the octupole parameter values $\kappa = 0$, 0.2, and 0.5. Dotted curve represent the quantum result, and the solid curve represent the semiclassical trace formula taking into account the contribution of some short regular polygon families confined in the sphere part of the cavity.

is ignored for simplicity. Taking into account the correct k dependence, one has another expression where the Gaussian is replaced by a different but similar single-peaked function (see Fig. 11 of Ref. [10]).

In this way, one can extract information on the contribution of classical POs by the Fourier transform of the quantum level density. The summation in Eq. (14) can be truncated at certain $k_{\max}$ if one takes k_c sufficiently smaller than $k_{\max}$. k_c determines the resolution ΔL of the orbit length by the uncertainty relation $\Delta L = 1/k_c$. Sufficiently large k_c is required for a good resolution of the orbit length, and I took $k_c R_0 = 20$ (R_0 being the radius of the potential in the spherical limit) and $k_{\max} = \frac{3}{2}k_c$ in the present calculation.

The upper panel of Fig. 6 displays the modulus of quantum-mechanical Fourier transform $|F^{(\mathrm{qm})}(L;\kappa)|$ as a function of the length variable L and the octupole parameter κ. In the lower panel, the length of the classical POs are plotted as functions of octupole parameter. Solid curves represent the lengths of the regular polygon POs confined in the sphere part of the potential, and broken lines represent those of the meridian-plane orbits. By comparing these two panels, it can be seen that the Fourier amplitude has strong peaks mainly along the orbit families confined in the sphere part. Particularly, the peak corresponding to the triangular orbit S(3, 1) is outstanding. Thus, one can expect that the gross shell effect is given mostly by the contribution of this triangular family.

The effect of the shell structure on deformation should be estimated by the shell energy, rather than the level density. Using Eq. (11), one obtains the trace formula for shell energy as [9,26]

$$\delta E(N) = \int^{e_F} (e - e_F)\delta g(e) de \simeq \sum_{\mathrm{PO}} \frac{\hbar^2}{T_{\mathrm{PO}}^2} A_{\mathrm{PO}}(e_F) \cos\left(k_F L_{\mathrm{PO}} - \frac{\pi}{2}\mu_{\mathrm{PO}}\right), \quad (16)$$

where $e_F = (\hbar k_F)^2/2M$ is the Fermi energy satisfying

$$N = \int^{e_F} g(e) de. \quad (17)$$

The additional factor T_{PO}^{-2} in Eq. (16) suppresses the contributions of longer orbits, and accordingly one has only to consider a few shortest POs with higher degeneracies.

For the cavity model under consideration, the contribution of the PO family confined in the sphere part can be directly evaluated by the trace formula for a truncated spherical cavity, which has been derived for the study of the nascent-fragment (prefragment) shell effect in nuclear fission processes [10]. Figure 7 shows the results of shell energies (16) for the octupole parameter values $\kappa = 0$, 0.2, and 0.5. For these relatively small octupole deformations, quantum results are nicely

reproduced by the contribution of POs confined in the sphere part of the potential. One finds that the oscillating pattern in case of the spherical shape survives well in the octupole deformed system.

Keeping in mind that the shell effect is essentially determined by the POs confined in the sphere part of the potential, let us consider the condition for the system to take the octupole shape by focusing attention on the PO contribution. Because of the saturation property, volume V surrounded by the potential surface is proportional to the particle number N. According to the Weyl's asymptotic formula [35], the leading term of the average level density is given by[1]

$$g_0(e) \simeq \frac{2M}{\hbar^2}\frac{Vk}{4\pi^2}, \tag{18}$$

with the volume

$$V = \frac{4\pi}{3}R_0^3 = \frac{4\pi}{3}Nr_0^3, \tag{19}$$

where $R_0 = N^{1/3}r_0$ is the nuclear radius in the spherical limit. From the relation between Fermi wave number k_F and particle number N, one obtains

$$N \simeq \int_0^{\hbar^2k_F^2/2M} g_0(e)de = \frac{Vk_F^3}{6\pi^2} \simeq \frac{2N(k_Fr_0)^3}{9\pi},$$
$$k_F \simeq \left(\frac{9\pi}{2}\right)^{1/3} r_0^{-1}.$$

Thus, the value of the Fermi wave number k_F is approximately independent of the particle number N.

In the trace formula (16), let us introduce the reduction factor $w_{\rm PO}$ of the PO family amplitude due to the truncation, and assume that the Maslov indices are unchanged by the truncation[2]

$$A_{\rm PO}(e_F) = w_{\rm PO}A_{\rm PO}^{(0)}(e_F), \quad \mu_{\rm PO} \simeq \mu_{\rm PO}^{(0)}, \tag{20}$$

where $A_{\rm PO}^{(0)}$ and $\mu_{\rm PO}^{(0)}$ represent the amplitude and Maslov indices for the PO family in the spherical cavity without truncation. Inserting them into Eq. (16) and replacing $w_{\rm PO}$ with w_{31} of the dominant triangular orbit S(3, 1), one has

$$\delta E(N) \simeq w_{31}\sum_{\rm PO}\frac{\hbar^2}{T_{\rm PO}^2}A_{\rm PO}^{(0)}\cos\left(k_FL_{\rm PO} - \frac{\pi}{2}\mu_{\rm PO}\right)$$
$$= w_{31}\delta E^{(0)}(N^{(0)}(e_F)), \tag{21}$$

where $\delta E^{(0)}$ is the shell energy of the spherical cavity without truncation. Since the number of the constituent particles is proportional to the volume surrounded by the potential surface under the fixed Fermi energy, one has

$$\frac{N^{(0)}(e_F)}{N} = \frac{V_{\rm sph}}{V} \equiv f(\kappa), \tag{22}$$

[1]The unit $\hbar^2/2M = 1$ is used in Ref. [35].

[2]To be precise, one has the small shifts of the Maslov indices due to the contribution of the marginal orbits which correspond to the higher-order quantum corrections [10].

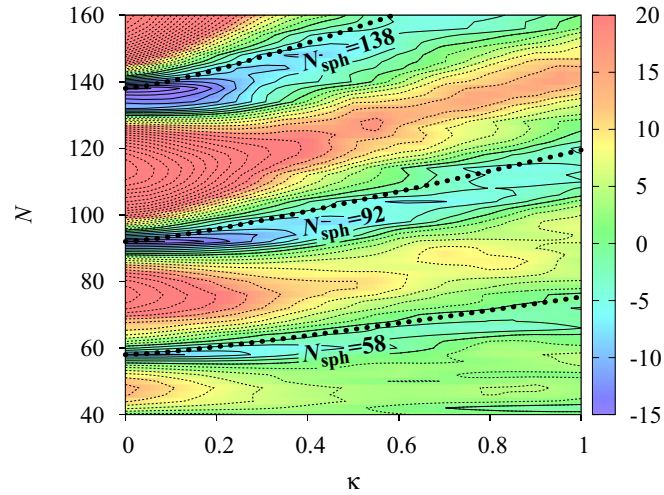

FIG. 8. Contour plot of the shell energies as functions of octupole parameter κ and particle number N. Solid and broken contour curves represent negative and positive shell energies, respectively. Thick dotted lines indicate where the radius of the sphere part of the potential is equal to the radius of spherical magic nuclei with $N_{\rm sph} = 58$, 92, and 138.

where V and $V_{\rm sph}$ are volumes of the total system and that of the sphere composing the octupole surface (1), $V_{\rm sph} = 4\pi a^3/3$. $f(\kappa)$ is a monotonically decreasing function of κ as easily presumed from Fig. 2. As displayed in Fig. 7, the expression of Eq. (21) with $N^{(0)}(e_F) = f(\kappa)N$ explains the main feature of the shell structure quite well.

According to the rough but meaningful estimation discussed above, the shell energy described by the contribution of PO in Eq. (16) is essentially governed by the lengths $L_{\rm PO}$ of the orbits in the sphere part of the potential. The contribution of the PO family confined in the sphere part of the potential will then give shell energy minima if the radius of the sphere part is identical to the radius of spherical magic nucleus. Figure 8 shows the contour plot of the shell energy in the (κ, N) plane. The curves $N = N_{\rm sph}/f(\kappa)$, obtained by substituting some spherical magic numbers $N_{\rm sph}$ for $N^{(0)}(e_F)$ in Eq. (22), are also drawn in the figure. One will find that those curves successfully explain the shell energy valleys.

IV. SUMMARY

Octupole deformation of nuclei above the spherical magic configurations are investigated by the simple cavity potential model, where the potential surface is parametrized by merging a sphere and a paraboloid. The semiclassical trace formula for the truncated spherical cavity is successfully applied to our model and gives us a clear understanding of the properties of shell structure. The contribution of a degenerate orbit family confined in the spherical subsystem brings about a strong shell effect similar to those in the spherical shape, and it plays a significant role in stabilizing the octupole shape. This mechanism nicely explains the systematics of the octupole deformations on the nuclear chart.

This result is also related to the recent works on the role of the octupole shape degree of freedom in fission fragments [36,37]. In the fission process, prefragments take octupole shapes near the scission point, and the octupole shell effect controls the size of the fragment. Since the systems with the number of particles a little above the spherical magic number prefer octupole deformation, it explains why the mass number of heavier fragments is concentrated around 140, a little larger than that of doubly magic ^{132}Sn.

The current shape parametrization can be generalized to spheroid+paraboloid, which enables us to investigate the ground state shapes of nuclei, taking account of the quadrupole and octupole shape degrees of freedom. Results of the systematic analysis with such an extension will be discussed in a separate paper [18].

There have been various approaches to examine the ground-state octupole deformation over the nuclear chart, and in most of those analyses, axially symmetric type of octupole deformation was the main consideration. In this work, I have also limited myself to the axially symmetric case. However, it should be mentioned that nonaxial octupole shape degrees of freedom and the role of $\Delta l = 3$ pair of levels in it were analyzed, and a pronounced bunching of levels was found in the case of Y_{32} deformation, which has tetrahedral symmetry [7,8]. The theoretical search of tetrahedral nuclei has been extensively carried out with the realistic mean field model [38,39]. Recently, all four types of octupole shapes and the role of the point-group symmetries were examined in Pb and superheavy regions [40,41].

In the present work, the axially symmetric octupole deformation for the nuclei just above the spherical shell closures is shown to be related to the dynamical symmetry, which can be taken as a partial survival of the spherical symmetry for special combination of quadrupole and octupole deformations. On the other hand, a strong tetrahedral shell effect is expected by the bifurcation of PO on the way from spherical to larger tetrahedral deformation [42]. It is an interesting subject to investigate the systematics of nonaxial octupole deformations over the nuclear chart and its semiclassical origin, which is left for future work.

ACKNOWLEDGMENTS

I would like to thank Prof. Kenichi Matsuyanagi for his helpful comments and discussions. Part of the numerical calculations in this work were carried out at the Yukawa Institute Computer Facility.

[1] P. A. Butler and W. Nazarewicz, Rev. Mod. Phys. **68**, 349 (1996).
[2] P. Möller, R. Bengtsson, B. Carlsson, P. Olivius, T. Ichikawa, H. Sagawa, and A. Iwamoto, At. Data Nucl. Data Tables **94**, 758 (2008).
[3] L. M. Robledo and G. F. Bertsch, Phys. Rev. C **84**, 054302 (2011).
[4] S. E. Agbemava, A. V. Afanasjev, and P. Ring, Phys. Rev. C **93**, 044304 (2016).
[5] Y. Cao, S. E. Agbemava, A. V. Afanasjev, W. Nazarewicz, and E. Olsen, Phys. Rev. C **102**, 024311 (2020).
[6] S. Ebata and T. Nakatsukasa, Phys. Scr. **92**, 064005 (2017).
[7] I. Hamamoto, B. R. Mottelson, H. Xie, and X. Z. Zhang, Z. Phys. D: At. Mol. Clusters **21**, 163 (1991).
[8] F. Frisk, I. Hamamoto, and F. R. May, Phys. Scr. **50**, 628 (1994).
[9] V. M. Strutinsky and A. G. Magner, Sov. J. Part. Nucl. **7**, 138 (1976).
[10] K. Arita, Phys. Rev. C **98**, 064310 (2018).
[11] K. I. Arita, T. Ichikawa, and K. Matsuyanagi, Phys. Rev. C **98**, 064311 (2018).
[12] K. Arita, T. Ichikawa, and K. Matsuyanagi, Phys. Scr. **95**, 024003 (2020).
[13] U. Mosel and H. W. Schmitt, Nucl. Phys. A **165**, 73 (1971).
[14] U. Mosel and H. W. Schmitt, Phys. Rev. C **4**, 2185 (1971).
[15] C. L. Zhang, B. Schuetrumpf, and W. Nazarewicz, Phys. Rev. C **94**, 064323 (2016).
[16] J. Sadhukhan, C. l. Zhang, W. Nazarewicz, and N. Schunck, Phys. Rev. C **96**, 061301(R) (2017).
[17] S. Frauendorf and V. V. Pashkevich, Ann. Phys. (Berlin) **508**, 34 (1996).
[18] K. Arita, arXiv:2304.00655.
[19] T. Mukhopadhyay and S. Pal, Nucl. Phys. A **592**, 291 (1995).
[20] W. D. Heiss, R. G. Nazmitdinov, and S. Radu, Phys. Rev. Lett. **72**, 2351 (1994).
[21] K. Arita and K. Matsuyanagi, Nucl. Phys. A **592**, 9 (1995).
[22] A. Sugita, K. Arita, and K. Matsuyanagi, Prog. Theor. Phys. **100**, 597 (1998).
[23] K. Arita, Phys. Scr. **91**, 063002 (2016).
[24] M. C. Gutzwiller, J. Math. Phys. **12**, 343 (1971).
[25] R. Balian and C. Bloch, Ann. Phys. (NY) **69**, 76 (1972).
[26] M. Brack and R. K. Bhaduri, *Semiclassical Physics* (Westview, Boulder, 2003).
[27] K. Arita, Phys. Rev. C **86**, 034317 (2012).
[28] M. V. Berry and M. Tabor, Proc. R. Soc. London A **349**, 101 (1976).
[29] S. C. Creagh and R. G. Littlejohn, Phys. Rev. A **44**, 836 (1991).
[30] H. Schomerus and M. Sieber, J. Phys. A: Math. Gen. **30**, 4537 (1997).
[31] A. G. Magner, S. N. Fedotkin, K. Arita, T. Misu, K. Matsuyanagi, T. Schachner, and M. Brack, Prog. Theor. Phys. **102**, 551 (1999).
[32] A. G. Magner and K. Arita, Phys. Rev. E **96**, 042206 (2017).
[33] B. K. Jennings, Ann. Phys. **84**, 1 (1974).
[34] P. Ring and P. Schuck, *The Nuclear Many-Body Problems* (Springer, New York, 1980).
[35] R. Balian and C. Bloch, Ann. Phys. (NY) **60**, 401 (1970).
[36] G. Scamps and C. Simenel, Nature (London) **564**, 382 (2018).
[37] G. Scamps and C. Simenel, Phys. Rev. C **100**, 041602(R) (2019).
[38] J. Dudek, A. Goźdź, N. Schunck, and M. Miśkiewicz, Phys. Rev. Lett. **88**, 252502 (2002).
[39] J. Dudek, D. Curien, I. Dedes, k. Mazurek, S. Tagami, Y. R. Shimizu, and T. Bhattacharjee, Phys. Rev. C **97**, 021302(R) (2018).

[40] J. Yang, J. Dudek, I. Dedes, A. Baran, D. Curien, A. Gaamouci, A. Góźdź, A. Pędrak, D. Rouvel, H. L. Wang, and J. Burkat, Phys. Rev. C **105**, 034348 (2022).

[41] J. Yang, J. Dudek, I. Dedes, A. Baran, D. Curien, A. Gaamouci, A. Góźdź, A. Pędrak, D. Rouvel, and H. L. Wang, Phys. Rev. C **106**, 054314 (2022).

[42] K. I. Arita and Y. Mukumoto, Phys. Rev. C **89**, 054308 (2014).